High-Order Numerics in an Unstaggered Three-Dimensional Time-Split Semi-Lagrangian Forecast Model

L. M. LESLIE

Bureau of Meteorology Research Centre, Melbourne, Australia

R. J. PURSER

Meteorological Office, Bracknell, England

(Manuscript received 2 July 1990, in final form 18 January 1991)

ABSTRACT

Traditional finite-difference numerical forecast models usually employ relatively low-order approximations on grids staggered in both the horizontal and the vertical. In a previous study, Purser and Leslie (1988) demonstrated that high-order differencing on an unstaggered horizontal grid led to improved forecast accuracy. The present investigation has two aims. The first aim simply is to extend the earlier work to a three-dimensional formulation, by using high-order horizontal numerics in a time-split, three-dimensional, semi-Lagrangian model on a grid that is unstaggered in both the horizontal and vertical. The choice of an unstaggered grid is very effective in a semi-Lagrangian model as it ensures that a single set of interpolations suffices for all variables at each advection step. The second aim specifically is to increase the accuracy of the vertical discretization of key quantities such as the vertically integrated divergence, and the computation of the geopotential from the hydrostatic equation. Errors introduced in these terms potentially can have a large impact on the forecast accuracy. The increased accuracy also serves to mitigate any possible deterioration that might result from the adoption of a vertically unstaggered grid.

It is shown over a four-month period of daily 24-h forecasts that the use of *vertical quadrature* techniques, on the aforementioned terms, based on layer integrals of high-order interpolating Lagrange polynomials, leads to a significant reduction of about 5% in the root-mean-square errors of the geopotential and wind fields. A much greater improvement in model performance is found in the forecasts of vertical velocity and precipitation fields, as they are more sensitive to the new vertical discretization. Moreover, these gains are obtained at minimal computational cost both in time and storage.

1. Introduction

The history of numerical weather prediction (NWP) has largely been preoccupied with methods for reducing errors in the model forecasts. This endeavor has been very successful, with model errors steadily being reduced, and the useful lifespan of global forecasts correspondingly increasing to the present level of about five to six days. The increase in accuracy has come from a number of sources: a better specification of the initial state as more data have become available; the introduction of data assimilation techniques that make greater use of the additional data; the continued development of initialization procedures; greatly increased resolution owing to the availability of modern supercomputers; and improved representation of important physical processes that occur in the atmosphere.

To the above list should also have been added the use of high-order differencing techniques in the horizontal, which are capable of providing improved accuracy in the resolvable scales at relatively small cost. Hitherto, however, there has been very little interest shown in high-order differencing schemes and they have had only a relatively limited role in mainstream numerical forecasting centers despite the recognition of their potential value early in the history of NWP (see, for example, Gerrity 1973), and at various other times over the years (Kalnay-Rivas and Hoitsma 1977; Campana 1979).

Part of the reason for the lack of interest shown in high-order differencing schemes was that they are difficult to introduce on the staggered grids that most forecast centers currently employ. Recently, however, Purser and Leslie (1988) have argued that the questions of unstaggered grids and high-order differencing should be handled jointly. We demonstrated that with the use of higher-order differencing in the horizontal, the unstaggered grid (or Arakawa A grid, as it is usually referred to) was a very attractive grid because of the ease with which high-order operators could be introduced. Considerable gains in accuracy follow the introduction of such operators, at very little computational cost

Corresponding author address: Dr. Lance M. Leslie, BMRC, GPO Box 1289K, Melbourne Victoria 3001, Australia.

compared with the drastic increase in computing power required by increasing the model resolution.

If the arguments for the use of high-order differencing operators in the *horizontal* are accepted, the next immediately obvious question to be asked is whether the introduction of high-order numerics in the *vertical* would also have a significant impact on the accuracy of the model forecasts. This is a particularly interesting question because forecast failures that occur in the current numerical forecast models sometimes are related to errors in the vertical discretization. In particular, forecasts of precipitation patterns and amounts can be very sensitive to the vertical differencing scheme used.

In this study we present a time-split three-dimensional semi-Lagrangian limited-area forecast model on a grid that is unstaggered in both the horizontal or the vertical, and that has high-order accurate numerics in the vertical as well as the horizontal. High-order accurate schemes in the vertical have been investigated by other authors, but usually in the form of finite-element schemes based on the Galerkin approach (Staniforth and Daley 1979; Burridge et al. 1986; Steppeler 1986). Our model employs sixth-order horizontal numerics but, rather than using a Galerkin finite-element procedure in the vertical, it achieves high-order accuracy (again, up to sixth-order) simply by using vertical quadrature based on Lagrange interpolation polynomials to obtain vertical motion from the horizontal divergence and geopotential from the temperature.

A particularly strong motivation for this study was the special advantages the unstaggered grid holds for semi-Lagrangian methods. The semi-Lagrangian technique was introduced into barotropic primitive-equation models by Robert (1982) as a means of overcoming the advective restriction on the time-step size in a semi-implicit formulation (see also Staniforth and Temperton 1986). The technique has since been extended to multilevel models (see, for example, Robert et al. 1985; McDonald 1986) and has been shown to be beneficial in split-explicit models (Bates 1984). In a semi-Lagrangian model the motivation for using an unstaggered grid is particularly strong: a staggered arrangement of variables necessitates the duplication, or even tripling, of grid interpolations; or a compromise of numerical consistency by interpolating all variables as if they are coincident, or by other averaging procedures. As none of these alternatives has much appeal we argue below in the section on vertical discretization for the use of unstaggered grids to preserve numerical accuracy.

The forecast model is run on the Australian region analysis archives on a daily basis for the four-month period 1 July 1989–31 October 1989, producing a total of 123 24-h forecasts. The major aim of the study is to assess the significance of introducing high-order numerics in the vertical by comparing the performance of the sixth-order scheme with a standard, second-order scheme.

2. Model equations

a. Governing equations

Using the Phillips (1957) vertical coordinate $\sigma = p/p_s$, the governing equations can be written as

$$\frac{dU}{dt} = fV - \frac{\partial \phi}{\partial x} - RT\frac{\partial}{\partial x}\ln p_s + D_U, \tag{2.1}$$

$$\frac{dV}{dt} = -fU - \frac{\partial \phi}{\partial y} - RT\frac{\partial}{\partial y}\ln p_s + D_V, \tag{2.2}$$

$$\frac{d}{dt}\ln p_s = \frac{\partial \dot{\sigma}}{\partial \sigma} - m^2\left(\frac{\partial U}{\partial x} + \frac{\partial V}{\partial y}\right), \tag{2.3}$$

$$\frac{dT}{dt} = \frac{RT}{C_p}\left(\frac{d}{dt}\ln p_s + \frac{\dot{\sigma}}{\sigma}\right) + \frac{D_T}{C_p} \tag{2.4}$$

$$\frac{Dq}{Dt} = D_q \tag{2.5}$$

$$\frac{\partial \phi}{\partial \sigma} = -\frac{RT}{\sigma}, \tag{2.6}$$

where $U = u/m$, $V = v/m$; m is the map factor for the Lambert conformal projection of the Australian region (local derivatives of m may be neglected); p and p_s are the pressure and surface pressure; and the remaining terms have their usual meanings.

b. Vertical discretization

As mentioned in the Introduction, and as will be described in detail in section 3, in this study a grid that is unstaggered in both the horizontal and the vertical will be used. In a previous article, Purser and Leslie (1988) have shown that by using a combination of high-order spatial differencing and selective low-pass filtering it is possible to overcome the well-documented difficulties (see, for example, Mesinger 1981) associated with the unstaggered horizontal grid. The grid is especially attractive for a semi-Lagrangian model because it means that only one family of trajectories and their corresponding interpolation coefficients need to be computed.

Similar considerations apply also to the vertical, except that the cumulative distortion of the small-scale structure by advection is quite minor (presumably due to the inhibiting and restorative effects of thermal stratification), enabling us to dispense with filters to control noise in the vertical. Therefore, we chose to use a three-dimensional unstaggered arrangement of the σ levels at which all variables, including $\dot{\sigma}$, are held.

Hitherto, vertical differencing schemes have been selected largely on the grounds that they preserve some of the conservation properties of the continuous equa-

tion, such as momentum, kinetic energy, and total potential energy. Tokioka (1978) evaluated eight different kinds of vertical discretization, including the unstaggered grid, which he rejected along with a number of other grids as being inadequate. Later studies by Arakawa and Suarez (1984) and Arakawa (1988) presented arguments in favor of the so-called "Lorenz" grid (where $\dot{\sigma}$ is staggered relative to U, V, and T), which maintains many of the conservation properties of the continuous system. The Lorenz grid has long been favored by NWP modelers and, as Bleck (1984) has stated, "is by far the most common vertical differencing and advection scheme in large-scale modeling."

The unstaggered grid has not been a popular choice among NWP modelers because holding $\dot{\sigma}$ at the same levels as U and V implies, for a given order of accuracy, an increase of truncation errors in treating the continuity equation, particularly for structures at the limit of the vertical resolution of the grid. However, particularly in the case of semi-Lagrangian schemes, the unstaggered grid is particularly advantageous for the treatment of vertical advection in two ways: first, the collocation of $\dot{\sigma}$ and the other model variables obviates the need for vertical averaging of $\dot{\sigma}$ in trajectory calculations. This is because the full wind vector (U, V, $\dot{\sigma}$) is needed in the three-dimensional semi-Lagrangian model; second, the employment of high-order vertical numerics can readily be introduced to reduce the truncation errors. We note here a comment by one of the reviewers that in the Lorenz grid the correct hydrostatic coupling between collocated ϕ and T also is inherently difficult to represent accurately for grid-scale structures, so that high-order numerics would be advantageous for the Lorenz grid as well.

The above considerations, together with a desire to achieve consistency in the horizontal and vertical, prompted us to choose the simplest means of deploying the variables—namely, the unstaggered grid—and to use *high-order quadrature* to reduce the truncation errors associated with deriving ϕ from RT/σ in the hydrostatic equation (2.6), and computing $\dot{\sigma}$ from the continuity equation (2.3).

The *quadrature formulas* are based on layer integrals of the interpolating polynomials of the prescribed degree. Details of the scheme are given in the Appendix. Away from the top and bottom boundaries the interpolation templates are centered on the target intervals and involve as many levels as the nominal order of accuracy; immediately adjacent to the boundaries the templates shrink to avoid inaccuracies associated with the "overshooting" often incurred by one-sided polynomial interpolations. Considering the hydrostatic equation as an example, with sigma levels σ_m, the interpolated value of $\partial\phi/\partial\sigma$ is found from the Lagrange formula [see Eqs. (A.1) and (A.2) in the Appendix] and integrated within each model layer. Relating $\partial\phi/\partial\sigma$ to temperature by Eq. (2.6) at each level leads to the quadrature formula

$$\Delta\phi_k \equiv \phi_{k+1} - \phi_k \approx -\sum_m Q(k, m)\frac{RT_m}{\sigma_m}, \quad (2.7)$$

$$\equiv \sum_m \mathrm{VQUAD}\phi(k, m)T_m, \quad (2.8)$$

where VQUADϕ is the vertical quadrature coefficient for ϕ. A corresponding formula is used to construct each layer increment $\Delta\dot{\sigma}_k$ of $\dot{\sigma}$ from the vertical integral of horizontal mass divergence within the layer and the rate of change of surface pressure.

c. *Accuracy of the quadrature schemes and vertical modes*

A 13-layer model was used in this study. The actual model levels chosen were,

$$\sigma_n = 0.02 + 0.08 \times (n - 1), \quad n = 1, \cdots 13$$

and

$$\sigma_{14} = 1.0. \quad (2.9)$$

It is important to note that this distribution of levels is far from ideal for resolving internal inertia-gravity waves uniformly: this would require a greater concentration of levels in the upper part of the atmosphere, as shown by Baer and Ji (1989). However, especially in a short-range regional forecast model, the tropospheric perturbations are of primary interest while the inertia-gravity waves present in a dynamically balanced model are of the forced, nonpropagating kind, and are present essentially to maintain quasi-geostrophic balance. Therefore, the shapes of the vertical modes in the upper regions, where they are poorly represented, are not expected to resemble those of the exact modes of corresponding equivalent depths. Lower down in the atmosphere, where the model resolution given by (2.9) theoretically is adequate, we are much more justified in using the model vertical modes as the natural dynamical structures to assess the accuracy of the quadrature schemes applied to the hydrostatic and continuity equations.

The vertical modes of the 13-layer model are found by linearizing Eqs. (2.1)–(2.6) relative to a basic vertical temperature profile $T_0(\sigma)$ in the usual manner. Vertical modes are then found for the following vertical quadrature schemes: (i) second-order; (ii) nominal fourth-order, and (iii) nominal sixth-order. In the latter two cases, the formal order of accuracy becomes less than the nominal order at the top and bottom of the model atmosphere.

The upper boundary condition in the model is

$$\dot{\sigma}_1 = 0. \quad (2.10)$$

This boundary condition, while simple, is arbitrary: other boundary conditions are equally justifiable and yet will lead to different discrete spectra of equivalent

depths (the real spectrum of internal modes should be continuous).

Vertical modes emerging from the linearized "test" model using the three schemes (i)–(iii) are not expected to be directly comparable with the corresponding modes of a high-resolution model employing boundary condition (2.10) because of the aforementioned distortions of modal structures at high altitudes. Therefore, we compute instead the modes of a high-resolution model with the "tunable" mode-dependent upper boundary condition generalizing Eq. (2.10).

$$\dot{\sigma}_1 + \beta \frac{\partial}{\partial t} \ln p_s = 0 \qquad (2.11)$$

with β tuned independently for each method (i)–(iii), and each mode, to ensure an exact match of equivalent depths. This numerical device allows a fairer comparison among the coarse resolution methods by not penalizing them simply because their spectra of equivalent depths happen not to coincide with the spectrum from a model that can resolve the upper strata. Table 1 lists the spectrum of equivalent depths of the linearized model for each of the quadrature schemes.

Figure 1 shows the thermal profile used as the basic state for the computation of the normal modes. The profile is given by the idealized formula:

$$T_0(\sigma) = 225 + \frac{65}{2(1-\sigma_a)} \{(\sigma - \sigma_a) + [\sigma_b^2 + (\sigma - \sigma_a)^2]^{1/2}\}, \qquad (2.12)$$

where $\sigma_a = 0.3$, $\sigma_b = 0.1$.

Figure 2 shows the first, third, and sixth vertical modes using the second-order quadrature. Profiles are shown together for the horizontal wind and temperature perturbation, along with the corresponding "exact" modes computed using at least three times the vertical resolution and a fourth-order method, but "tuned" by the upper boundary condition (2.11) to possess identical equivalent depths as in the second-order quadrature.

As anticipated, deviations between the modal profiles of the "exact" and the "test" model become apparent first at the upper levels, then amplify and extend downward as the modal index increases. Beyond mode 6 the comparison becomes meaningless, as the modes are as much "computational" as "physical." Figures 3 and 4 show the sixth vertical mode for the fourth- and sixth-order methods, respectively, and should correspond with Fig. 2c. While it is clear that the exact modes are incapable of being resolved at the upper levels, the fit between the exact and test modes is preserved to higher altitudes as the nominal order of accuracy increases from second through to sixth.

It should be stated clearly that the main value of the above exercise is to remind us that grid-scale perturbations are not likely to be treated faithfully, even at high orders of accuracy, but also to show that the correspondence is closer for scales that are within the effective resolution of the vertical discretization when higher-order schemes are used. The major aim of this study, namely, a convincing demonstration of the value of high-order vertical discretization involves a comprehensive assessment of the performance of the second- and sixth-order schemes in a fully nonlinear primitive-equation model using real data. Such a model is described in the next section.

3. The forecast model

The forecast model used in the numerical experiments was a 13-layer primitive-equation model on the Australian region analysis–forecast domain. The model details are described immediately below.

a. Horizontal discretization

As discussed in section 2, the horizontal differencing was carried out on an unstaggered grid using high-order operators. Sixth-order operators were selected, on a grid of horizontal resolution 100 km. The grid dimensions were 100 × 60 points. The particular horizontal differencing operators employed are described in detail by Purser and Leslie (1988), which also includes an assessment of their accuracy relative to lower-order differencing on staggered grids.

b. Time discretization

The governing equations are solved using a two-time-level split semi-Lagrangian scheme. The procedure consists of a semi-Lagrangian advection step with time step Δt_s followed by N adjustment steps with time step $\Delta t_s = N\Delta t_a$. (A final, "physics," step is carried out to calculate D_u, D_v, etc., and is discussed briefly in section 3e).

TABLE 1. Equivalent depths in nearest whole meters of the 13-level test model using second-, fourth- and sixth-order vertical quadrature.

Quadrature order	1	2	3	4	5	6	7	8	9	10	11	12
Second	9515	1433	289	81	31	12	5	2	1	0	0	0
Fourth	9397	1531	331	99	39	16	7	3	1	0	0	0
Sixth	9401	1525	346	110	43	18	8	3	1	0	0	0

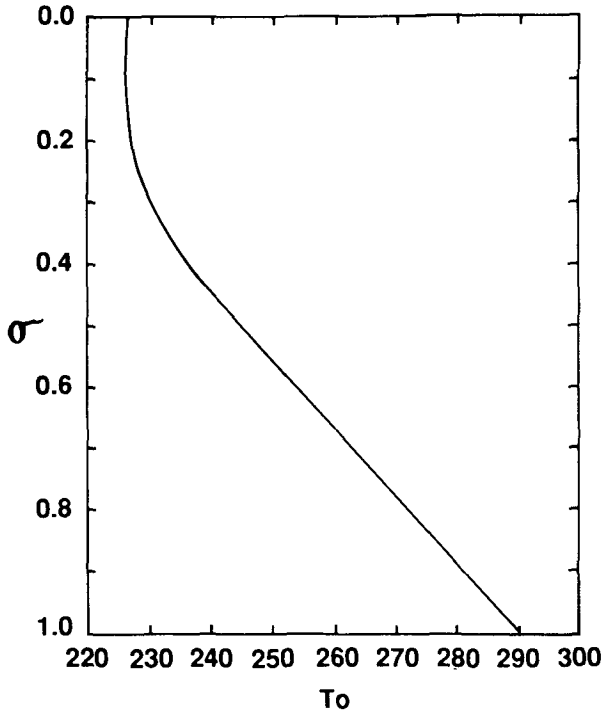

FIG. 1. Basic-state temperature profile used in computing vertical normal modes.

1) THREE-DIMENSIONAL SEMI-LAGRANGIAN ADVECTION

The semi-Lagrangian discretization of the momentum, thermodynamic, continuity, and moisture equations is given by

$$\frac{DU}{Dt} = 0, \tag{3.1}$$

$$\frac{DV}{Dt} = 0, \tag{3.2}$$

$$\frac{DT}{Dt} = 0, \tag{3.3}$$

$$\frac{D}{Dt}(\ln p_s) = 0, \tag{3.4}$$

$$\frac{Dq}{Dt} = 0, \tag{3.5}$$

where all the variables are as defined in section 2, above and,

$$\frac{D}{Dt} = \frac{\partial}{\partial t} + m^2\left(U\frac{\partial}{\partial x} + V\frac{\partial}{\partial y}\right) + \dot{\sigma}\frac{\partial}{\partial \sigma}.$$

The semi-Lagrangian procedure is similar to that described by Tanguay et al. (1989) in which an iterative procedure is used to calculate the three-dimensional displacements. As found by Tanguay et al. only two, and sometimes three, iterations are required. The values of the variables at the departure point are calculated using a sixth-order three-dimensional interpolation scheme.

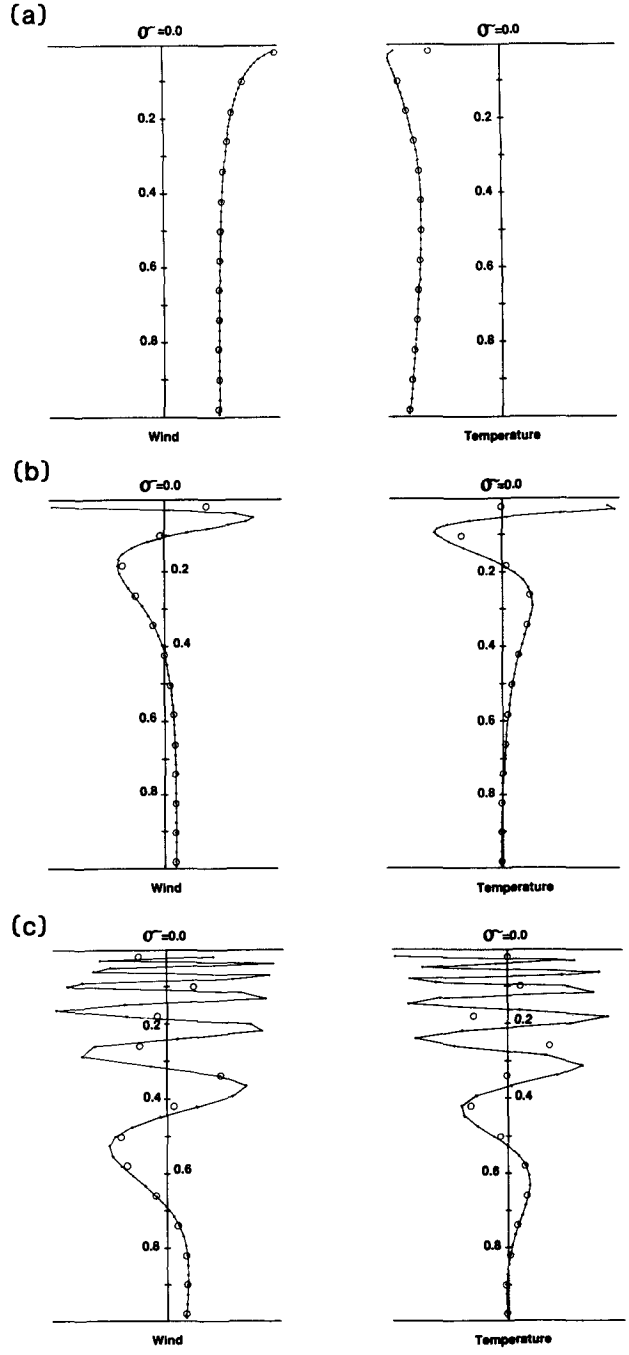

FIG. 2. A selection of vertical normal modes of the basic state shown in Fig. 1, using second-order quadrature in the hydrostatic and continuity equations: (a) mode 1 (external mode); (b) mode 3; (c) mode 6. The circles depict values from the 13-layer test model. The continuous curves are accurately computed modes (using a 46-level model) of precisely the same equivalent depths and normalized so as to coincide with the 13-layer wind mode at the lowest level.

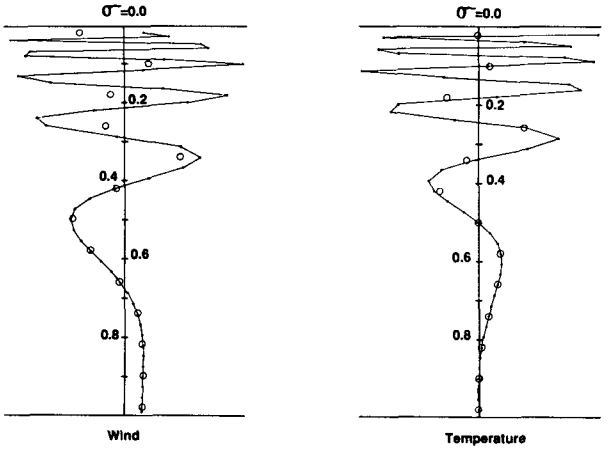

FIG. 3. As for Fig. 2c, but using fourth-order vertical quadrature.

An important feature of the scheme is that, following McGregor (1986), the advective change in the surface pressure field, $\ln p_s$, is saved at each model level. That is,

$$Ap_s = -m^2\left(U\frac{\partial}{\partial x}\ln p_s + V\frac{\partial}{\partial y}\ln p_s\right),$$

is calculated from the semi-Lagrangian method and stored. Except in the linear terms of the adjustment equations, p_s itself is not updated until the geostrophic adjustment procedure is carried out.

2) ADJUSTMENT STEP

The commonly used forward–backward scheme (Mesinger 1977) is used for the adjustment step. Defining the divergence D by

$$D = m^2\left(\frac{\partial U}{\partial x} + \frac{\partial V}{\partial y}\right), \tag{3.6}$$

the adjustment equations become

$$\frac{\partial}{\partial t}\ln p_s = \frac{1}{(1-\sigma_1)}\int_{\sigma_1}^{1}(Ap_s - D)d\sigma, \tag{3.7}$$

$$\dot{\sigma} = (1-\sigma)\frac{\partial}{\partial t}\ln p_s + \int_1^{\sigma}(Ap_s - D)d\sigma', \tag{3.8}$$

$$\frac{\partial T}{\partial t} = \frac{R}{C_p\sigma}\frac{\omega}{p_s}T, \tag{3.9}$$

$$\frac{\omega}{p_s} = \dot{\sigma} + \sigma\left(\frac{\partial}{\partial t}\ln p_s - Ap_s\right), \tag{3.10}$$

$$\phi = \phi_s - \int_1^{\sigma}\frac{RT}{\sigma'}d\sigma', \tag{3.11}$$

where ϕ_s is the surface geopotential,

$$\frac{\partial U}{\partial t} = fV - \frac{\partial \phi}{\partial x} - RT\frac{\partial}{\partial x}\ln p_s, \tag{3.12}$$

$$\frac{\partial V}{\partial t} = -fU - \frac{\partial \phi}{\partial y} - RT\frac{\partial}{\partial y}\ln p_s. \tag{3.13}$$

The forward–backward scheme is applied by solving Eqs. (3.7)–(3.11) for $\ln p_s$, ω, T, and ϕ. The latest values of these variables are then used in Eqs. (3.12) and (3.13) to calculate new values of U and V. The Coriolis terms are treated implicitly. The adjustment step is repeated N times and then the semi-Lagrangian procedure is applied again, and so on until the end and the forecast period is reached.

In this study an adjustment time step $\Delta t_a = 5$ min was used and the number of adjustment steps per semi-Lagrangian step was chosen to be $N = 4$. Values of N up to 6 were experimented with, but had minimal effect on the forecasts and the more conservative value was used.

c. Vertical discretization

As discussed in section 2 above, the quadrature formula (2.8) and the corresponding one for the continuity equation are used instead of the conventional vertical differencing schemes, in the computation of the geopotential, ϕ, from the hydrostatic equation, and the vertical velocities $\dot{\sigma}$ and ω from the continuity equation.

d. Lateral boundary conditions

Because the model is a limited area model, a lateral boundary condition scheme must be used. In this study, the current operational procedure is employed; that is,

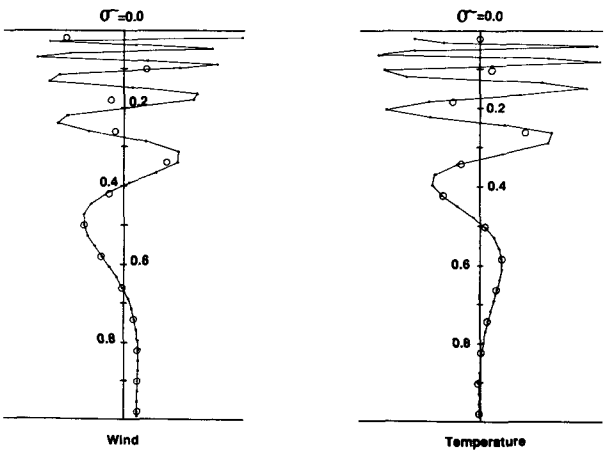

FIG. 4. As for Fig. 2c, but using sixth-order vertical quadrature.

a weighted average of the archived operational hemispheric forecast and the limited-area model forecast. The weighting function is linear and drops from 1.0 to 0.0 over five grid points.

e. *Parameterization of physical processes*

The representation of physical processes in the forecast model is very similar to that of the Australian Bureau of Meteorology's current operational model. It is described in full detail by Leslie et al. (1985) and only a brief description will be given here. The parameterization of vertical turbulent exchanges of momentum, heat, and moisture are based on a stability-dependent surface layer and mixing-length theory above the surface layer. Parameterization of precipitation consists of two successive adjustments: large-scale condensation when there is stable ascent, and the mixing ratio exceeds 95% of the saturation value; and a modified Kuo cumulus convection scheme when there is large-scale moisture convergence and conditional instability present. Evaporation of falling precipitation is allowed for. Finally, there is a surface heat budget with a prediction equation for the surface temperature, using a 3-level soil model.

f. *Analysis/initialization*

The operational objective analysis scheme used by the Bureau of Meteorology is based on that of Mills and Seaman (1990). Mean sea-level pressure and geopotential layer thicknesses are analyzed using a two-dimensional univariate statistical interpolation, and each wind component is analyzed using a three-dimensional univariate statistical interpolation scheme. Temperature and dewpoint are analyzed using the successive correction method. The mass and wind fields are mutually adjusted using variational techniques.

The initialization scheme used is the vertical mode initialization scheme developed by Bourke and McGregor (1983).

4. Numerical experiments

In this section the models being compared will be referred to as the V6 (sixth-order vertical quadrature) and V2 (second-order) models, respectively.

TABLE 2. Mean rms errors at a selection of the standard pressure levels for the models V6 and V2, respectively. The geopotential rms errors are in decameters and the wind rms errors are in meters per second.

Field	Geopotential		Wind	
Pressure level	V6	V2	V6	V2
250 hPa	5.0	5.3	10.4	10.9
500 hPa	2.9	3.1	6.4	6.7
850 hPa	2.5	2.7	5.1	5.4

TABLE 3. Subjective assessment for the 123-day period 1 July–31 October of precipitation forecasts from the V6 and V2 models, respectively.

V6 superior	V6 inferior	Little difference	Total
54	22	47	123

a. *Data*

The model described in section 3 was run once each day on 0000 UTC data for the period 1 July–31 October inclusive, a total of 123 24-h forecasts. This particular period was notable for a higher than average number of cold fronts and cutoff cyclones crossing southern Australia. These meteorological events are of great significance to southern Australia because they are responsible for most of the winter and spring rainfall.

b. *Verification*

The forecasts from the V6 and V2 models were compared using the operational verification procedure that computes root-mean-square (rms) differences between the forecasts and the verifying analyses. In addition, because we are comparing models with different vertical dynamics, an attempt was made to compare the precipitation forecasts and vertical velocity fields. A hybrid "subjective/objective" procedure was used in which senior forecasters rated the precipitation forecasts from the two models in terms of intensity, location, and pattern, against the Australian rainfall gage network over the land, and against satellite imagery over the oceans. The forecasters had no knowledge of which forecast was which.

c. *Results*

1) RMS ERRORS

The rms errors for the V6 and V2 models were compiled and are tabulated in Table 2 at a selection of standard pressure verification levels used by the operational system. In the case of the geopotential, the percentage improvement in accuracy of the V6 model over the V2 model is 6%, 4%, and 5% at 850, 500, and 250 hPa, respectively. The corresponding improvements in the rms wind errors are 6%, 5%, and 6%, respectively. These are significant gains in skill, given that they result entirely from the vertical discretization.

2) PRECIPITATION FORECAST

The comparative performance of the V6 and V2 models is summarized in Table 3. In contrast with the relatively modest reductions in rms errors obtained

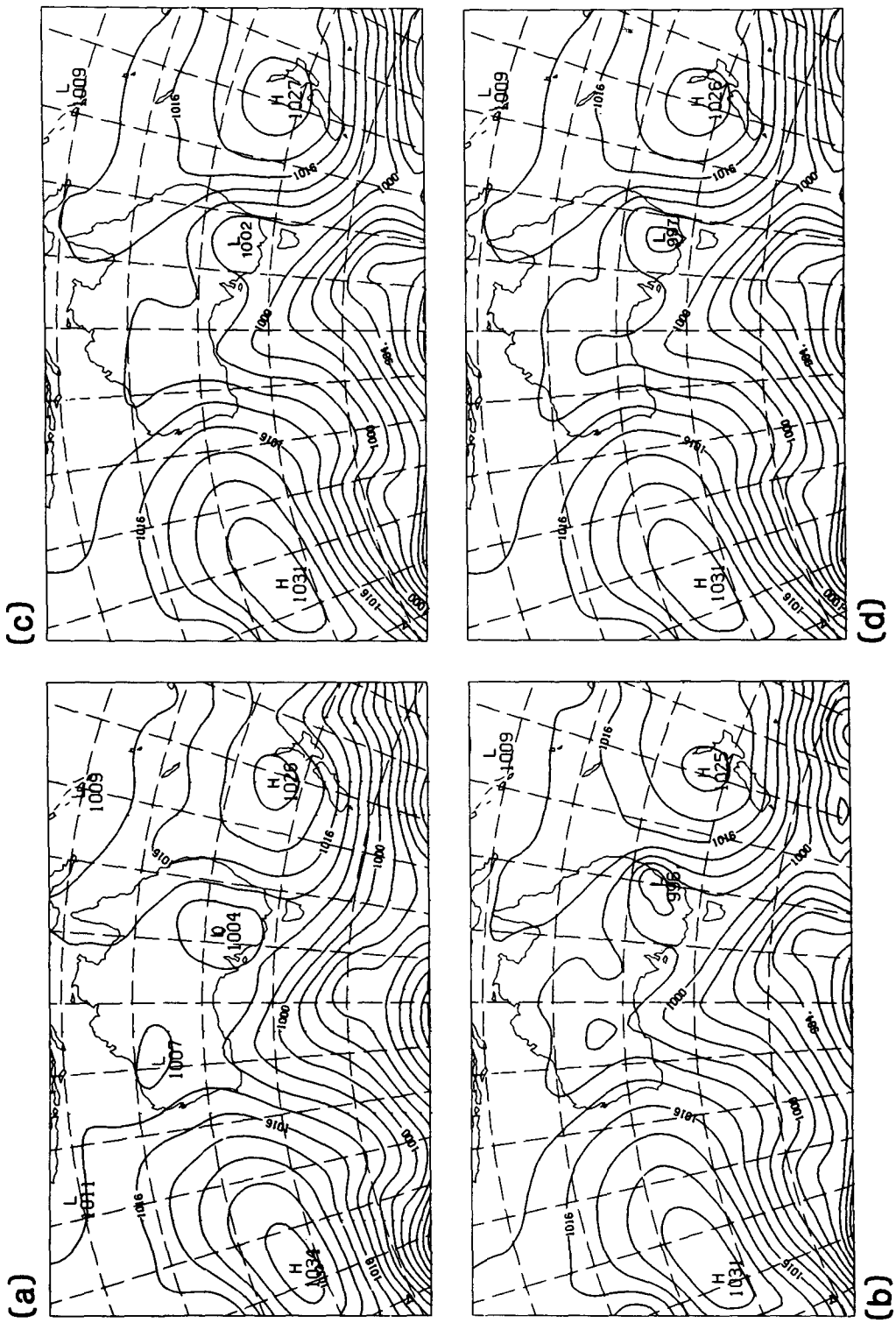

FIG. 5. Case study for the 24-h period 0000 UTC 24 October–0000 UTC 25 October 1989. (a) Initial mean sea-level pressure analysis; (b) verifying analysis; (c) 24-h forecast without vertical quadrature; (d) 24-h forecast using vertical quadrature.

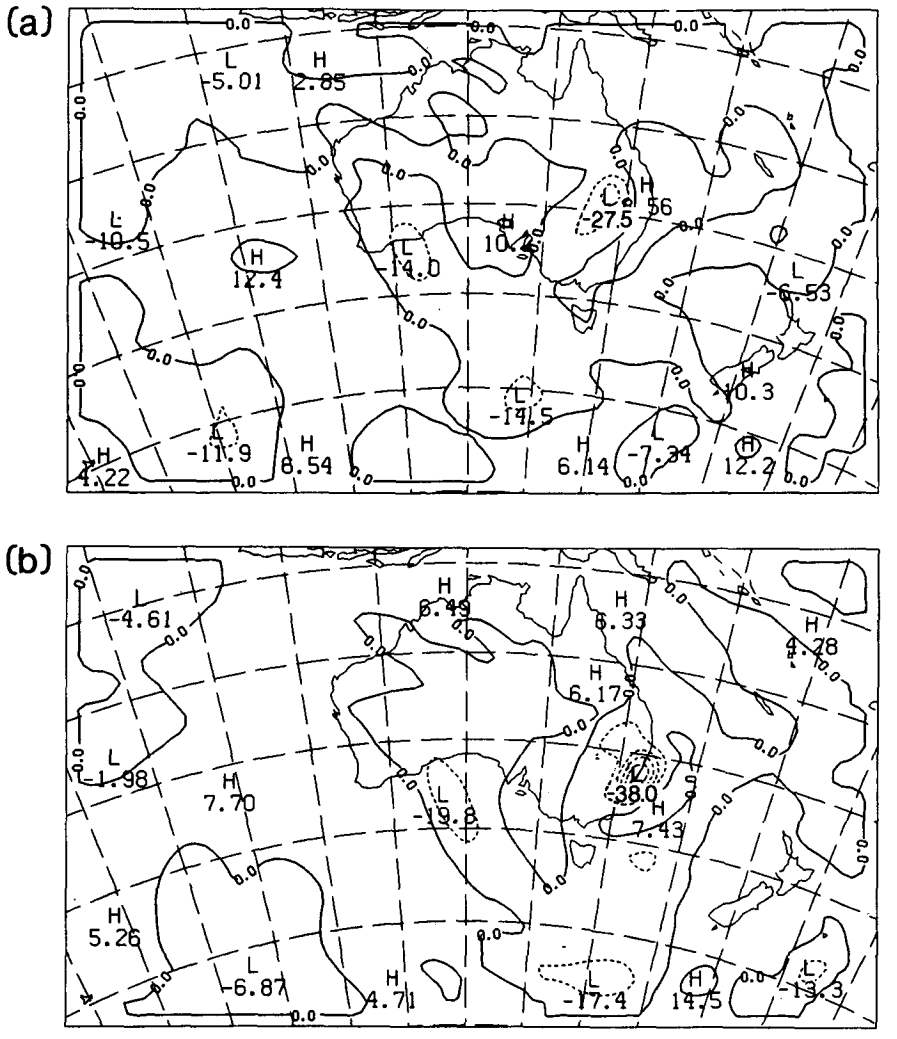

FIG. 6. Comparison of 24-h forecast 700-hPa vertical velocity field ω (hPa h^{-1})
(a) without vertical quadrature; (b) with vertical quadrature.

from the V6 model, in this case the V6 model performance equaled or outperformed the V2 model on 101 of the 123 cases, that is, on 82% of occasions. This is an especially encouraging result, and an example of an improved rainfall prediction case will be given below.

3) MODEL TIMINGS

The Bureau of Meteorology is an operational NWP center and high levels of computational efficiency are required of its models. The CPU time required by the model was changed very little by the introduction of high-order operators in the vertical. The timings, averaged over 10 model runs, on the Bureau's CRAY X-MP14 were 214 and 220 seconds per model day, respectively, for the V2 and V6 models, a very modest increase of 2.8%. This small increase is due largely to the ease with which the "numerics" vectorizes. In contrast, the model "physics" is difficult to vectorize and takes more than 60% of the total CPU time. This adds further weight to the advantages of high-order operators. If the vertical differencing scheme was modified simply by adding more grid points to a standard second-order scheme, the number of points at which the physics would be applied increases, and with it the computational time required by the model.

d. Case study

To illustrate the possible forecast improvements that can be obtained from the use of the sixth-order quadrature scheme, a case study is presented, for the 24-h period 0000 UTC 24–25 October 1989, in which there are two main features of interest, both of which were unusually prevalent in 1989. These are the frontal system traversing the Southern Ocean waters to the south

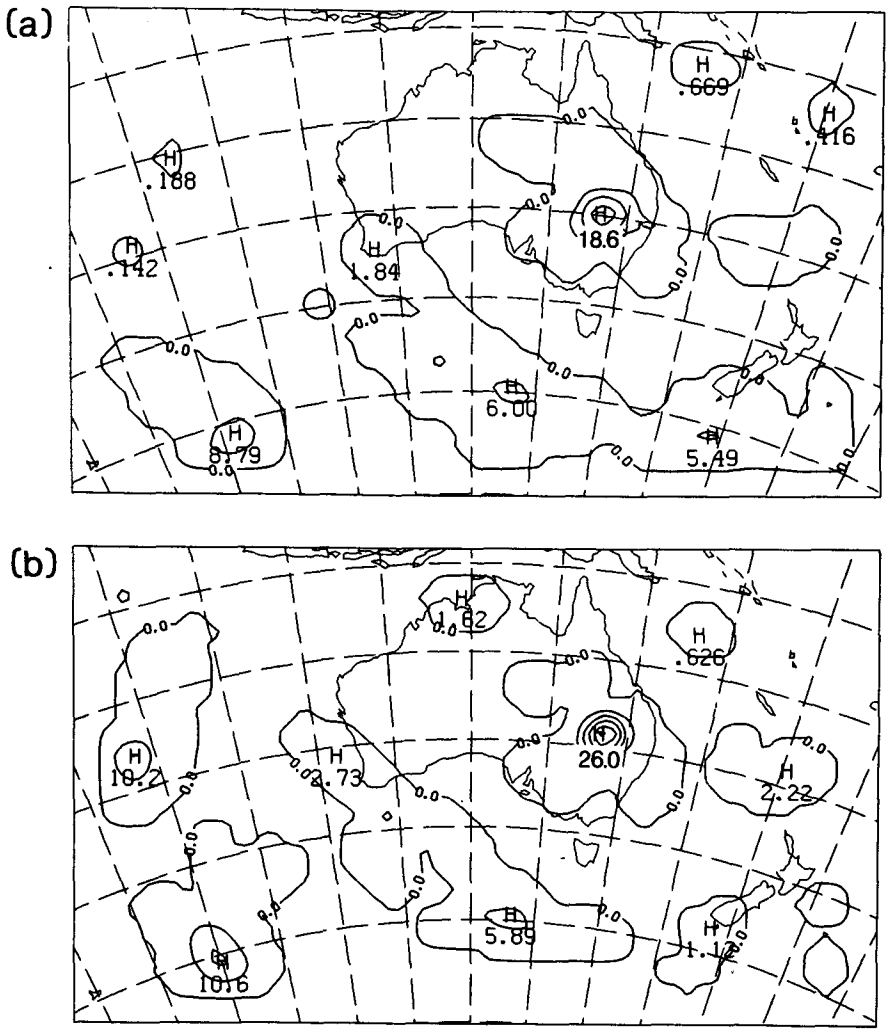

FIG. 7. As in Fig. 6, except for 24-h precipitation (mm).

of Western Australia, and the cutoff cyclone over southeastern Australia (see Fig. 5a). Twenty-four hours later the frontal system had continued its progress eastward, and the cutoff low had deepened significantly from 1004 to 996 hPa, as shown in Fig. 5b. The V2 model forecast predicted the position of the front quite well but decreased the central pressure of the cutoff low by only 2 hPa (see Fig. 5c). In contrast, the V6 forecast, although having little impact on the frontal system, produced a dramatically better forecast of the cutoff low, deepening it to a central value of 997 hPa, as shown in Fig. 5d.

This case study was deliberately chosen not to be the most spectacular example but to be representative of that group of significantly improved predictions obtained by the sixth-order quadrature scheme, in this type of situation. Apart from the mean sea-level pressure forecasts, the other major impact was on the vertical velocity and precipitation fields, particularly those associated with the cutoff low. A comparison of Figs. 6a,b show that the vertical velocities are much higher with the V6 forecast, with the maximum upward value of ω increasing from 27.5 to 38.0 hPa h^{-1}. The precipitation associated with the cutoff low also has been increased from a maximum of 18.6 to 26.0 mm (see Figs. 7a,b. Observed values in the region were greater than 25 mm, confirming the superiority of the forecast using sixth-order vertical quadrature.

5. Conclusions

It has been shown that replacing the second-order vertical discretization scheme by a higher-order quadrature technique in a finite-difference NWP model by a quadrature technique, which is described in section 2 and in the Appendix of this paper, leads to gains in

accuracy when verified over a large number of cases. These gains usually are reflected in larger vertical velocities in active systems such as cold fronts and developing cyclones, in higher rainfall totals and more realistic precipitation patterns, and also in lower rms errors in the wind and geopotential fields. In some individual cases, one of which is presented in detail in section 4, major improvements can be obtained in events for which accurate predictions of the vertical motion field are required. In this particular case the forecast using the sixth-order vertical quadrature produced an excellent forecast of a heavy rainfall event whereas the standard second-order vertical discretization scheme was relatively poor.

Overall, there was a reduction in rms errors in the wind field of about 6% and in the geopotential height of about 5% relative to observations at stations on the Australian continent. However, as already mentioned, the gains were much larger on some occasions and the values and patterns of the vertical velocity and precipitation fields frequently exhibited quite pronounced improvement.

Finally, the above-mentioned gains were achieved at very little computational cost. On a vector machine the additional time required to compute the higher-order scheme is small, and the calculations do not require additional storage as the number of grid points is not altered in higher-order schemes.

Acknowledgments. We would like to express our gratitude to Diann Vale and Lily Gao for typing the manuscript and to David Pike for assistance in preparing the diagrams. We would also like to thank the senior forecasters at the National Meteorological Centre, Melbourne, for their help in the assessment of the rainfall forecasts.

The work was partially supported by the U.S. Office of Naval Research under Grant N-000014-89-J-1737.

APPENDIX

Derivation of Formulas for Vertical Interpolation, Differencing, and Quadrature

The Lagrange interpolation polynomial for a generic variable ψ at level σ from N data points ψ_i stored at model levels σ_i, $i \in [J_1, J_2]$ (where $J_2 = J_1 + N - 1$), takes the form

$$\psi(\sigma) = \sum_{i=J_1}^{J_2} I_i(\sigma)\psi_i, \tag{A.1}$$

where

$$I_i(\sigma) = \prod_{j \neq i, j \in [J_1, J_2]} \frac{\sigma - \sigma_j}{\sigma_i - \sigma_j}. \tag{A.2}$$

Since each $I_i(\sigma)$ is a polynomial in σ of degree $N - 1$, it may be differentiated at σ to yield the corresponding coefficient of *the vertical differencing operator,*

$$D_i(\sigma) = \frac{dI_i(\sigma)}{d\sigma}, \tag{A.3}$$

such that

$$\frac{\partial \psi}{\partial \sigma}(\sigma) = \sum_{i=J_1}^{J_2} D_i(\sigma)\psi_i. \tag{A.4}$$

Likewise, each polynomial $I_i(\sigma)$ may be integrated between successive levels σ_n, σ_{n+1}, in order to yield the corresponding coefficient of the *quadrature formula* for this interval that uses the specified N data ψ_i:

$$\int_{\sigma_n}^{\sigma_{n+1}} \psi(\sigma)d\sigma = \sum_{i=J_1}^{J_2} Q_i\psi_i, \tag{A.5}$$

$$Q_i = \int_{\sigma_n}^{\sigma_{n+1}} I_i(\sigma)d\sigma. \tag{A.6}$$

For a nominal order of accuracy of $2M$, the limits J_1, J_2, of the templates used for quadrature or interpolation in $[\sigma_n, \sigma_{n+1}]$ are

$$J_1 = \max(1, n + 1 - M),$$
$$J_2 = \min(N_{\text{lev}} + 1, n + M), \tag{A.7}$$

where N_{lev} is the number of model levels and "level $N_{\text{lev}} + 1$" denotes the ground ($\sigma = 1$). Where ψ is a variable not explicitly stored at the ground, an effective value is substituted for $\psi_{N_{\text{lev}}+1}$ by linearly extrapolating from the two lowest levels [e.g., the horizontal divergence used in the continuity equation (3.8)]. The corresponding limits in the case of vertical differencing at σ_n are

$$J_1 = \max(1, n - M),$$
$$J_2 = \min(N_{\text{lev}}, n + M). \tag{A.8}$$

Truncating the templates at the top and bottom means that the actual order of accuracy is formally less than the nominal, at least for nominally fourth- and sixth-order schemes. In practice, however, the degradation of accuracy due to such truncations is not significant but, were it ever to be found so, a simple remedy would be to draw the levels closer together at the top and bottom.

REFERENCES

Arakawa, A., 1988: Finite-difference methods in climate modelling. *Physically-Based Modelling of Climate and Climate Change,* M. E. Schlesinger, Ed., Kluwer Academic Publishers, 169–221.

——, and V. R. Lamb, 1977: Computational design of the basic

dynamical processes of the University of California Los Angeles general circulation model. *Methods of Computational Physics,* Vol. 17, J. Chang, Ed., Academic Press, 174–265.

——, and M. J. Suarez, 1984: Vertical differencing of the primitive equations in sigma coordinates. *Mon. Wea. Rev.,* **111,** 34–45.

Baer, F., and M. Ji, 1989: Optimal vertical discretization for atmospheric models. *Mon. Wea. Rev.,* **117,** 391–406.

Bates, J. R., 1984: An efficient semi-Lagrangian and alternating direction implicit method for integrating the shallow water equations. *Mon. Wea. Rev.,* **112,** 2033–2047.

Bleck, R., 1984: Vertical coordinate systems and differencing schemes. *Lectures Presented at the Workshop on Limited-Area Numerical Weather Prediction Models for Computers of Limited Power.* Errice, Italy, W.M.O., 169–174.

Bourke, W. P., and J. L. McGregor, 1983: A nonlinear vertical mode initialization scheme for a limited area prediction model. *Mon. Wea. Rev.,* **111,** 1749–1771.

Burridge, D. M., J. Steppeler and R. Strüfing, 1986: Finite element schemes for the vertical discretization of the ECMWF forecast model using linear elements. ECMWF Tech. Rep. No. 54, 80 pp. [Available from ECMWF, Shinfield Park, Reading, England.]

Campana, K. A., 1979: Higher order finite-differencing experiments with a semi-implicit model at the National Meteorological Center. *Mon. Wea. Rev.,* **109,** 18–36.

Gerrity, J. P. Jr., 1973: Numerical advection experiments with higher order, accurate, semimomentum approximations. *Mon. Wea. Rev.,* **101,** 231–234.

Kalnay-Rivas, E., and D. Hoitsma, 1979: Documentation of the fourth-order GLAS model. NASA Tech. Memo 80608, 126 pp. [Available from Goddard Space Flight Centre, Greenbelt, MD 20771.]

Leslie, L. M., G. A. Mills, L. W. Logan, D. J. Gauntlett, G. A. Kelly, M. J. Manton, J. L. McGregor and J. M. Sardie, 1985: A high resolution primitive equations model for operations and research. *Aust. Meteor. Mag.,* **33,** 11–35.

McDonald, A., 1986: A semi-Lagrangian and semi-implicit two time-level integration scheme. *Mon. Wea. Rev.,* **114,** 824–830.

McGregor, J. L., 1986: Accuracy and initialization of a two-level split semi-Lagrangian scheme. *Short and Medium-Range Numerical Weather Prediction,* T. Matsuno, Ed., Tokyo 100, Meteor. Soc. Jpn, 233–246.

Mesinger, F., 1977: Forward–backward scheme and its use in a limited-area model. *Contrib. Atmos. Phys.,* **50,** 200–210.

——, 1981: Horizontal advection schemes of a staggered grid—an enstrophy and energy conserving model. *Mon. Wea. Rev.,* **109,** 467–478.

Mills, G. A., and R. S. Seaman, 1990: The BMRC regional data assimilation system. *Mon. Wea. Rev.,* **118,** 1217–1237.

Phillips, N. A., 1957: A coordinate system having some special advantages for numerical forecasting. *J. Meteor.,* **14,** 184–185.

Purser, R. J., and L. M. Leslie, 1988: A semi-implicit, semi-Lagrangian finite-difference scheme using high-order spatial differencing on a nonstaggered grid. *Mon. Wea. Rev.,* **116,** 2069–2080.

Robert, A., 1982: A semi-Lagrangian and semi-implicit numerical integration scheme for the primitive meteorological equations. *J. Meteor. Soc. Jpn,* **60,** 319–325.

——, T. L. Yee and H. Ritchie, 1985: A semi-Lagrangian and semi-implicit integration scheme for multilevel atmospheric models. *Mon. Wea. Rev.,* **113,** 388–394.

Staniforth, A., and R. Daley, 1979: A baroclinic finite-element model for regional forecasting with the primitive equations. *Mon. Wea. Rev.,* **107,** 107–121.

——, and C. Temperton, 1986: Semi-implicit, semi-Lagrangian integration schemes for a barotropic finite-element regional model. *Mon. Wea. Rev.,* **114,** 2078–2090.

Steppeler, J., 1986: Finite element schemes for the vertical discretization of the ECMWF forecast model using quadratic and cubic elements. ECMWF Tech. Rep. No. 55, 59 pp. [Available from ECMWF, Shinfield Park, Reading, England.]

Tanguay, M., A. Simond and A. Staniforth, 1989: A three-dimensional semi-Lagrangian scheme for the Canadian Regional finite-element forecast model. *Mon. Wea. Rev.,* **117,** 1861–1871.

Tokioka, T., 1978: Some considerations on vertical differencing. *J. Meteor. Soc. Jpn,* **56,** 98–111.